

Two-fluid Model of Biofilm Disinfection

N. G. Cogan *

*Department of Mathematics, Florida State University, email: cogan@math.fsu.edu.
Supported by NSF award DMS-0612467

N. G. Cogan
Department of Mathematics
Florida State University
208 Love Building
Tallahassee, FL 32306
email: cogan@math.fsu.edu
Final Submission: Latex

Abstract

We consider a dynamic model of biofilm disinfection in two dimensions. The biofilm is treated as a viscous fluid immersed in a fluid of less viscosity. The bulk fluid moves due to an imposed external parabolic flow. The motion of the fluid is coupled to the biofilm inducing motion of the biofilm. Both the biofilm and the bulk fluid are dominated by viscous forces, hence the Reynolds number is negligible and the appropriate equations are Stokes equations.

The governing partial differential equations are recast as boundary integral equations using a version of the Lorenz reciprocal relationship. This allows for robust treatment of the simplified fluid/biofilm motions. The transport of nutrients and antimicrobials, which depends directly on the velocities of the fluid and biofilm, is also included. Disinfection of the bacteria is considered under the assumption that the biofilm grows slowly compared to the time-scale of diffusion/advection.

Keywords: Biofilm, Two-Fluid, Boundary Integral Method, Regularized Stokeslets

1 Introduction

Because of the many health, environmental and industrial processes that are impacted by bacteria biofilms, understanding the failure of antimicrobial treatments is of paramount importance. Currently there are several hypothesis concerning tolerance mechanisms that include phenotypic, environmental and structural mechanisms [10, 23, 30, 19]. Because it is likely that all of the mechanisms play some role in conferring tolerance mathematical models have been introduced to investigate these mechanisms [1, 5, 3, 14, 32, 13].

In this investigation, we expand a previous continuum model of biofilm disinfection [5] to include the coupled motion of the biofilm and the external fluid. In part, this is an important step in the development of a continuum model of disinfection that includes the material properties of the biofilm. However, we also find another mechanism that alters the effectiveness of antimicrobial treatment. We find that the motion of the biofilm can alter the killing effectiveness of continuous dosing. This effect depends on the relative viscosities of the fluid/biofilm materials as demonstrated by simulations comparing the killing curves for varying biofilm viscosities. We also demonstrate the dependance of the efficiency on the initial biofilm geometry with simulations comparing ideal geometries.

The manuscript is organized as follows: The first section gives an overview of the model and numerical implementation. This has been described previously in more detail [4] so the description will be relatively brief. We then describe the numerical simulations and comparisons. We conclude with a discussion and summary of the results.

2 Model Description

2.1 Overview

The fundamental simplification that we make in this investigation concerns the material properties of the biofilm. It is well known that the biofilm exhibits viscoelastic properties; however, the dominant behavior depends on the time-scale of interest. For disinfection, this time scale is on the order of hours while the relaxation time for biofilms has been estimated on the order of seconds [18]. Therefore we treat the biofilm as a viscous fluid whose viscosity is much larger than that of the external bulk fluid. The length scale is set by a typical thickness of a biofilm which is on the order of 500 microns, the velocity scale depends on the experimental procedure. We are focusing our attention on low flow systems such as those in [32], which include experiments with slowly flowing external fluids. Using typical values for the velocities in these experiments and the viscosity of water as the reference viscosity, we find that the Reynolds number, which compares the inertial scales to the viscous scales, is much less than one. This indicates that the inertial terms are negligible and we will treat both the biofilm and the bulk fluid as viscous fluids governed by Stokes equations.

For each time-step we determine the fluid and biofilm velocities as described below. Once the fluid and biofilm velocities are determined, we compute the advection, diffusion and reaction of the chemical substances. Since the chemical constituents equilibrate rapidly, the chemical concentrations are assumed to be at quasi-steady-state. We note that the diffusion coefficient is reduced within the biofilm. This is handled as in [5]. In particular, because the biofilm/fluid interface is not sharp in general, the diffusion coefficient varies smoothly from the external fluid to the internal biofilm. We smooth the diffusion coefficient with a fixed transition region between the value in the bulk fluid and that in the biofilm. The transition region is calculated independent of the discretization. Finally the bacterial concentration is de-

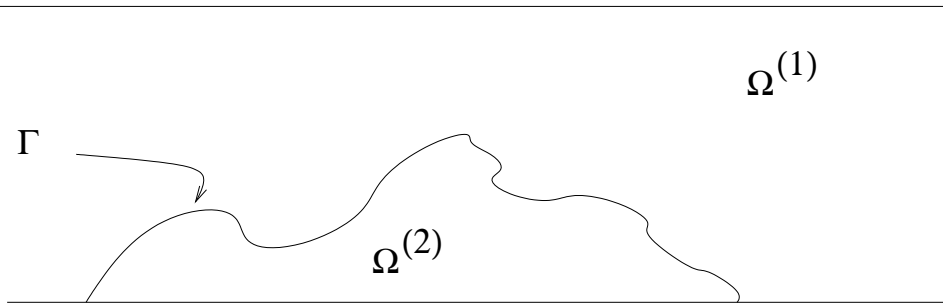


Figure 1: Schematic of the domain, Ω . The region is separated into two sub-regions, $\Omega^{(1)}$, the bulk fluid region, and $\Omega^{(2)}$, the biofilm region, by an interface Γ .

terminated by solving a conservation equation that includes disinfection and advection of the bacteria. Each of these equations and the numerical methods for approximating the solutions are described below.

2.2 Governing Equations

Bulk fluid and Biofilm Motion:

Because the time scale for the simulations is on the order of hours which is much less than the time scale for biofilm growth we also assume that the biofilm does not grow during the disinfection. Therefore both fluids are incompressible. The fluids occupy a region Ω , which is a channel for this manuscript, and are separated by a surface, Γ . We denote the two subregions as $\Omega^{(1)}$ and $\Omega^{(2)}$ for the bulk fluid and biofilm regions, respectively (see Figure 1).

The dynamics of both the bulk fluid and the biofilm are governed by the incompressible Stokes equations

$$\nabla \cdot \sigma^{(*)} = 0 \tag{1}$$

$$\nabla \cdot \mathbf{U}^{(*)} = 0, \tag{2}$$

where $* = 1, 2$ denotes variables in the bulk and biofilm regions, respectively. Stokes equations describe conservation of momentum and mass with stress tensors $\sigma^* = P^*\mathbf{I} + \mu^*(\nabla\mathbf{U}^* + \nabla\mathbf{U}^{*\mathbf{T}})$ contain both the hydrostatic pressures, P^* , and the viscous stresses proportional to the deformation gradient tensor.

There are several methods for treating the two fluid problem including immersed interface [20, 25, 22], immersed boundary [26] and the boundary

integral method [4, 8, 16, 28]. We choose to transform the equations governing the materials in each sub-domain, $\Omega^{(1)}$ and $\Omega^{(2)}$ (i.e. bulk fluid and biofilm) into a single integral equation whose solution is the velocity at each point in the domain. This method is referred to as the boundary integral method (BIM) and is described in more detail below. We will refer to the velocity of the system obtained using BIM as \vec{U} henceforth.

Constituents Disinfection of the bacteria within a biofilm depends on many factors. There have been numerous experimental [10, 14, 30, 15, 34, 23] and mathematical [31, 13, 32, 5] investigations of various biofilm resistance mechanisms. There is no consensus on the dominant mechanisms; however, because typical antimicrobial agents and antibiotics are most effective killing respiring bacteria [19] spatially dependent nutrient consumption leads to regions of lowered biocide effectiveness.

Because of the link between local nutrient availability and disinfection, accurate, realistic models of the dynamics of nutrient and antimicrobial concentrations must be considered. Since the diffusion of chemical constituents is fast compared to the time-scale of biofilm motion, we describe the concentrations of nutrient, $S(\vec{x}, t)$, and antimicrobial by reaction/diffusion/advection equations at quasi-steady-state,

$$\vec{U}(\vec{x}, t) \cdot \nabla S(\vec{x}, t) = \nabla \cdot (D_s \nabla S(\vec{x}, t)) - \mu_s \frac{S}{K_s + S} B(\vec{x}, t) \quad (3)$$

$$\vec{U}(\vec{x}, t) \cdot \nabla A(\vec{x}, t) = \nabla \cdot (D_a \nabla A(\vec{x}, t)) + R(A, B, S). \quad (4)$$

The diffusion coefficients of nutrient and antimicrobial agent, $D_s(\vec{x})$ and $D_a(\vec{x})$, are assumed to be smaller in the biofilm region than in the flow region with reduction factors are denoted r_s and r_a , respectively. The consumption of nutrient by the bacteria is modeled by Monod kinetics, where μ_s , Y_s and K_s denote the maximum specific growth rate, yield coefficient and Monod coefficient, respectively.

We note that the reaction term in Equation 4 depends on the antimicrobial agent being used since some agents are highly reactive with components of the biofilm. For this investigation we will assume that there is no reaction ($R == 0$) which implies that the antimicrobial agent equilibrates to the source concentration thus eliminating the need to compute the solution to Equation 4.

Bacteria The bacterial population at a point in space is changed by the advection of the biofilm as well as by disinfection at a rate that is propor-

tional to the substrate consumption. Combining these we find the equation governing the bacterial concentration is,

$$\frac{\partial B}{\partial t} + \nabla \cdot (\vec{U}B) = -\alpha \frac{S}{K_s + S} B(\vec{x}, t), \quad (5)$$

where B is zero outside the biofilm region. The coefficient α has adsorbed the antimicrobial source concentration.

2.3 Numerical Implementation

Velocities:

The boundary integral method (BIM) for treating fluid problems in various parameter regimes has been extensively studied in the past several decades. This method relies on the existence of a Green's function for the PDE operators. The immediate practicality of this method is apparent for fluids that can be treated as inviscid or as Stokes fluids [28, 16]. In either of these cases Greens functions for various domains are readily obtained.

The main idea behind BIM is to use a version of the Lorenz reciprocal relation [24] to recast the governing PDE's as boundary integrals equations. In general the reciprocal identity allows one to obtain information about a given flow, \mathbf{U} using information about another known flow, \mathbf{U}' . Because the flow field for a viscous fluid with a singular force can be calculated directly [7], we use this as the comparison flow. Once the reciprocal relation is derived the governing equations can be recast as integral equations whose domain is the boundary between the fluids.

We relate the unknown velocity \mathbf{U}^* to the flow induced by a singular force with intensity \mathbf{f} at a point \mathbf{x}_0 , \mathbf{U}' . Thus \mathbf{U}' is a fundamental solution to incompressible Stokes equations

$$\nabla \cdot \sigma' = \mathbf{f} \delta(\mathbf{x} - \mathbf{x}_0) \quad (6)$$

$$\nabla \cdot \mathbf{U}' = 0, \quad (7)$$

where $\sigma = -P\mathbf{I} + \mu(\nabla\mathbf{U} + \nabla\mathbf{U}^T)$. This is a convenient flow to use since the solution can be computed easily using Fourier transforms [27]. In two spatial dimensions the solution is

$$\begin{aligned} \mathbf{U}'(\mathbf{x}) &= -\frac{\mathbf{f}}{4\pi\mu} \ln(r) + (\mathbf{f} \cdot \mathbf{x}) \frac{\mathbf{x}}{4\pi\mu r^2} \\ &= -\frac{\mathbf{f}}{4\pi\mu} \mathbf{G}, \end{aligned} \quad (8)$$

where $r = \|\mathbf{x} - \mathbf{x}_0\|$ and \mathbf{G} is the two-dimensional Stokeslet. The corresponding pressure and stress tensor are

$$\begin{aligned} P' &= \frac{(\mathbf{f} \cdot \mathbf{x})}{2\pi r^2} \\ \sigma &= -\frac{\mathbf{f}}{4\pi\mu} \mathbf{T}. \end{aligned} \quad (9)$$

The reciprocal relation for the bulk flow is determined by relating solutions to Equations 1 and 2 to 6, 7. By direct calculation, we find that

$$\nabla \cdot (\mathbf{U}\sigma') - \nabla \cdot (\mathbf{U}\sigma) = \mathbf{f}\delta(\mathbf{x} - \mathbf{x}_0)\mathbf{U}, \quad (10)$$

which is the classical reciprocal relation.

Integrating the reciprocal relation, with various placements of the singular force, we recast Equations (1) and (2), with $* = 1$ as an integral equation whose domain is the interface Γ . The integral equation relates the bulk fluid velocity to the traction jump across the interface, denoted $\Delta\sigma = (\sigma^{(1)} - \sigma^{(2)})$, and the velocity (see [27] Chapter 5). The motion of the bulk fluid is

$$\begin{aligned} \mathbf{U}_j^{(1)}(\mathbf{x}_0) &= -\frac{1}{4\pi\mu^{(1)}} \int_{\Gamma} \Delta\sigma_{ik}\eta_k(\mathbf{x})\mathbf{G}_{ij}(\mathbf{x}, \mathbf{x}_0) dl(\mathbf{x}) \\ &\quad + \frac{1-\lambda}{4\pi} \int_{\Gamma} \mathbf{U}_i(\mathbf{x})\mathbf{T}_{ijk}(\mathbf{x}, \mathbf{x}_0)\eta_k(\mathbf{x}) dl(\mathbf{x}), \end{aligned} \quad (11)$$

where $\lambda = \frac{\mu^{(2)}}{\mu^{(1)}}$. Equation 11 governs the j -th component of the external fluid velocity.

In a similar manner, we obtain an integral equation for the motion in $\Omega^{(2)}$,

$$\begin{aligned} \mathbf{U}_j^{(2)}(\mathbf{x}_0) &= -\frac{1}{4\pi\mu^{(1)\lambda}} \int_{\Gamma} \Delta\sigma_{ik}\eta_k(\mathbf{x})\mathbf{G}_{ij}(\mathbf{x}, \mathbf{x}_0) dl(\mathbf{x}) \\ &\quad + \frac{1-\lambda}{4\pi\lambda} \int_{\Gamma} \mathbf{U}_i(\mathbf{x})\mathbf{T}_{ijk}(\mathbf{x}, \mathbf{x}_0)\eta_k(\mathbf{x}) dl(\mathbf{x}). \end{aligned} \quad (12)$$

These two integral equations govern the coupled motion of the external bulk fluid and the internal biofilm. Because the flows must be continuous at the boundary, we can obtain the boundary velocity by taking limit of 11 and

12 as \mathbf{x}_0 moves to the boundary. These limits both converge to

$$U_j(\mathbf{x}_0) = -\frac{1}{2\pi\mu^{(1)}(\lambda+1)} \int_{\Gamma} \Delta\sigma_{ik}\eta_k(\mathbf{x})\mathbf{G}_{ij}(\mathbf{x}, \mathbf{x}_0) dl(\mathbf{x}) + \frac{\kappa}{2\pi} \int_{\Gamma}^{\mathcal{PV}} \mathbf{U}_i(\mathbf{x})\mathbf{T}_{ijk}(\mathbf{x}, \mathbf{x}_0)\eta_k(\mathbf{x}) dl(\mathbf{x}), \quad (13)$$

where $\kappa = \frac{1-\lambda}{1+\lambda}$. The latter integral is an improper integral that must be handled with care. There are many methods for evaluating this integral that depend on the dimension of Γ as well as the kernel of the integral. In this situation, the singularity is integrable and straightforward quadrature rules work well [28].

To close the system in a straightforward manner we impose a constitutive relation relating the jump in traction, $\Delta\sigma_{ik}$ to mean curvature $\Delta\sigma = \gamma\eta\nabla \cdot \eta$ (see [27]).

One could use these equations to determine the velocity at each point in the domain; however, a more effective method has been developed in [4]. This method uses Equation 13 to determine the velocity of the interface. This, in turn, is used as data to determine forces that must be applied to the domain so that the material (fluid or biofilm) moves with the calculated velocities. These forces are then used to update the velocities. More details can be found in [4, 5]. Essentially, this hybrid method uses BIM to determine the boundary motion and the method of regularized Stokeslets to determine the velocity away from the boundary.

To solve Equation 13, we are then confronted with a system of coupled integral equations which can be written as

$$\mathbf{W} = \mathbf{b} + \frac{\kappa}{2\pi} \int_{\Gamma} \mathbf{K}\mathbf{W} dl(\mathbf{x}). \quad (14)$$

where $\mathbf{W} = (\mathbf{U}_1^{(1)}, \mathbf{U}_2^{(1)})$. The vector \mathbf{b} contains the Stokeslet and the tensor \mathbf{K} contains the related stress tensor, both of which are known.

A straightforward method for solving the discretized integral equations is Nystroms method [35] which requires a quadrature rule:

$$\int_a^b y(s)ds = \sum_{j=1}^n \omega_j y(s_j),$$

where ω_j denotes the weights of the quadrature rule. For our simulations we use Gauss-Legendre quadrature.

Both the vector \mathbf{b} and the kernel of the integral equation have integrable singularities. This can make naive Nystrom's method unstable. We choose to regularize these terms using the method of regularized Stokeslets. For this we solve the regularized version of the singular Stokes' equation

$$\nabla \cdot \sigma = \mathbf{f}_0 \phi_\epsilon(\mathbf{x} - \mathbf{x}_0) \quad (15)$$

$$\nabla \cdot \mathbf{U} = 0, \quad (16)$$

where $\phi_\epsilon(\mathbf{x} - \mathbf{x}_0)$ denotes a cutoff or *blob* function. There are many choices for the regularization term ϕ_ϵ that yield regularized Stokeslet and stress [7].

Once we have the regularized stresses we discretize the initial interface into n control points. We then solve Equation 14, with the vector \mathbf{b} and the kernel \mathbf{K} replaced with the regularized version.

Applying the quadrature rule to the regularized problem

$$\mathbf{W} = \mathbf{b}_\epsilon + \frac{\kappa}{2\pi} \int_\Gamma \mathbf{K}_\epsilon \mathbf{W} dl(\mathbf{x}), \quad (17)$$

yields a discrete system of the form

$$\mathbf{W}(\mathbf{x}_0) = \mathbf{b}(\mathbf{x}_0) + \frac{\kappa}{2\pi} \sum_{j=1}^n \mathbf{K}_\epsilon(\mathbf{x} - \mathbf{x}_0) \mathbf{W}(\mathbf{x}) \omega_j. \quad (18)$$

Evaluating this at the n control points leads to

$$\mathbf{W}(\mathbf{x}_{0,i}) = \mathbf{b}_{\mathbf{x}_{0,i}} + \frac{\kappa}{2\pi} \sum_{j=1}^n \mathbf{K}_\epsilon(\mathbf{x}_{0,i} - \mathbf{x}_j) \mathbf{W}(\mathbf{x}_{0,i}) \omega_j. \quad (19)$$

This system can be inverted using any convenient iterative solver (i.e. gmres or conjugate gradient). Once the velocities of the interface are calculated, we use techniques developed in [7] to obtain the velocities away from the interface. The boundary points are then moved at their prescribed velocity, a new boundary is determined and the process is repeated.

Constituents:

The steady-state nutrient concentration is determined numerically using ADI with second order-accurate upwinding to avoid excessive numerical diffusion. We note that the diffusion coefficient varies between the biofilm region and the bulk fluid region. This is primarily due to the restriction imposed by the polymeric component of the biofilm. Rather than treat the diffusion

coefficient as discontinuous, we smooth the values between D_{bulk} and $D_{biofilm}$ by a continuous approximation of the Heaviside function. Thus we have a smoothly varying diffusion coefficient. This allows for standard treatment of the diffusion/advection equation as well as yielding an approximation that is independent of the discretization. More details can be found in [5].

Bacterial Concentration: We use a simple implementation of the method of lines with second order upwinding and Matlab’s ode-suite to solve the discretized bacterial advection and disinfection equation. Thus we discretize the spatial component of the bacterial concentration, where the advection terms are given explicitly. This yeilds a system of ODE’s which are solved with a fourth order Runge-Kutta algorithm.

3 Simulations

It is often advantageous for bacteria to form biofilms either to evade predation (i.e. human immune system) [9] or to take advantage of alternative metabolic processes. In [18], the authors argue that the biofilms ability to react elastically to transient stresses and viscously to long term stresses allow the biofilm to stay in environmentally favorable environments while avoiding catastrophic material failures explains observed visco-elastic properties.

This investigation was motivated by the need to understand how biofilms protect the bacteria from disinfection. In particular, because the estimated viscosity of the biofilm is extremely high compared to that of the bulk fluid [18] we would like to understand what effect the viscosity of the biofilm has on disinfection. Although there are many possible tolerance mechanisms, we only include physiological tolerance (i.e. nutrient dependent disinfection) and delayed penetration through a diffusional barrier. We then compared the disinfection curves for varying biofilm viscosities

Since the biofilm moves with the fluid, one could argue that the motion of the biofilm should decrease the effectiveness of the disinfectant since the bacteria move away from the disinfectant. Alternatively, one could argue that as the dynamics of the geometry of the biofilm interface could increase the effectiveness since the surface area is enlarged as the biofilm moves with the fluid allowing for easier penetration of nutrient. In the absence of a compelling heuristic argument or experimental results mathematical modeling and simulations were used to address the question. Parameters for the simulations are given in Table 3.

| Parameter | Symbol | Units | Value | Source |
|--|-----------|---------------------------|-------------------------|---------|
| Maximum Specific Growth Rate | μ_s | h^{-1} | 0.417 | [31] |
| Yield Coefficient | Y_b | | 0.8 | [31] |
| Monod Coefficient | K_s | mg l^{-1} | 0.1 | [31] |
| Antimicrobial Agent Influent Concentration | C_a | mg l^{-1} | 5 - 20 | [31] |
| Nutrient Influent Concentration | C_s | mg l^{-1} | 10 | [31] |
| Nutrient Diffusion Coefficient | D_s | m^2h^{-1} | 9.67×10^{-6} | [31] |
| Antimicrobial Agent Diffusion Coefficient | D_s | m^2h^{-1} | 1.80×10^{-6} | [31] |
| Biofilm/Bulk Diffusivity Reduction | r_* | | 0.9 | [32] |
| Length Scale | L | m | 10^{-2} | Assumed |
| Max. Flow Rate | U_{max} | m h^{-1} | 0-3.4 | Assumed |
| Disinfection Rate Coefficient: | κ | | 0.4 | Assumed |
| Biofilm Viscosity | μ | cP | 1 - 1000 \times water | Assumed |

Table I: Parameters used in the simulations

Simulation 1: Generic Interface

In this set of simulations we consider the disinfection of a generic biofilm cluster whose initial geometry is shown in Figure 2. Survival curves were generated by simulating the effect of disinfection with a constant concentration of biocide and nutrient source. The survival of the bacteria is calculated by $\frac{\int B}{\int B_0}$, where B_0 is the initial concentration of bacteria. This gives the ratio of surviving bacteria as a function of time. We considered the effects of varying the viscosity of the biofilm over several orders of magnitude. In figure 3, we show the survival curves for various viscosities. As the viscosity increases, we see a decrease in the effectiveness of the disinfection. The survival curves converge to that of the fixed biofilm as the viscosity tends towards infinity. Apparently, the viscosity plays a role in the disinfection efficiency. In figures 4-7, we show the domain and contours of the nutrient concentrations for varying viscosities. We see that the nutrient is better able to penetrate the biofilm with lower viscosity. This seems to support the hypothesis that the expansion of the surface area increases the susceptibility of the bacteria. The next set of simulations examines disinfection for varying initial interfaces and fixed viscosity. Here we see the dependance of the disinfection on the initial geometry.

Simulation 2: Two Disjoint Hemispheres versus Triangle

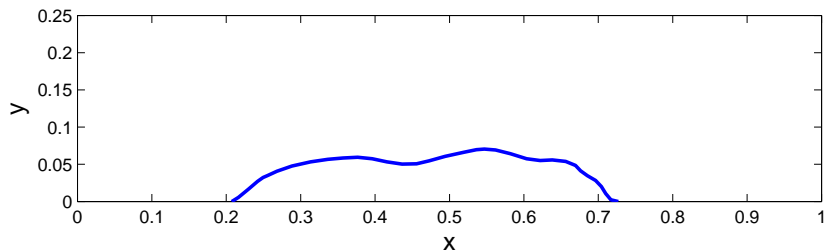


Figure 2: Initial generic interface used in Simulation 1.

We then simulated the disinfection for a biofilm with an interface that is initially two disjoint hemispheres of differing radii and compared the results with those obtained for two triangular regions (see Figure 8). Rather than vary the viscosity, we explored the results for different initializations of the interfaces. This was in part motivated by the observation that the lower viscosity generic interface seemed to be more 'streamlined' than the higher viscosity generic interface. Thus we consider whether the initial arrangement of the interface could be related to the effectiveness of disinfection. The results of these simulations are summarized in Figure 9.

Here we see that the interaction between the geometry and the advection/diffusion of chemical species is more complicated than just 'streamlining'. Intuitively, one would think that the relationship between effectiveness (i.e. time-scale of disinfection) would be similar between domains in column one and column two; however this is not the case. In Figure 10, we compare the arc lengths as a function of time for each of the domains. We see that even though the lower right of Figure 8 has larger arc length it is less

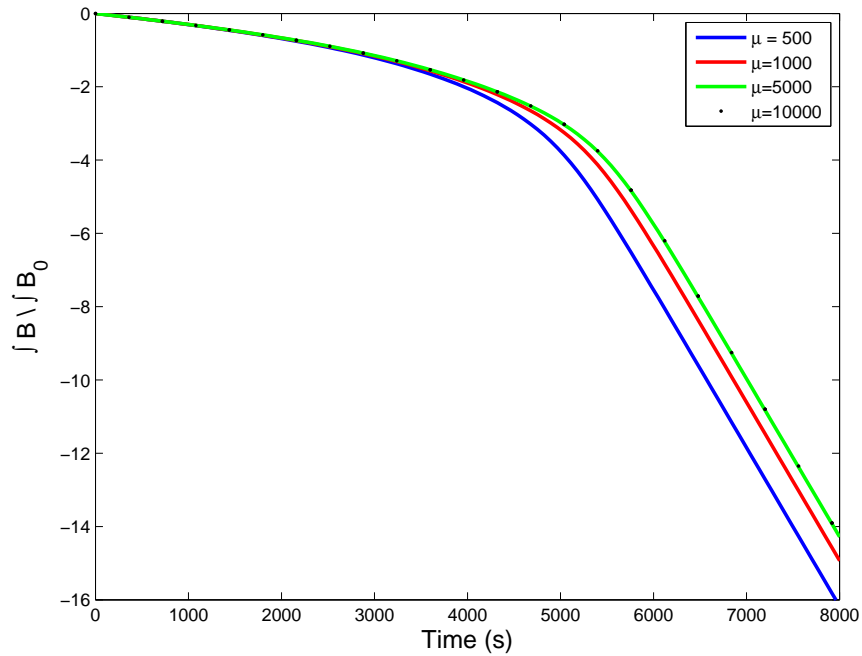


Figure 3: Comparisons of the survival curves for varying viscosities. As the viscosity increases, we see a delay in the disinfection indicating that the less viscous biofilms are more susceptible to treatment than the higher viscosity biofilms. We note that as the viscosity increases, the survival curves converge to that of the fixed biofilm domain as indicated by the overlap between the curves for $\mu = 5000$ and $\mu = 10000$.

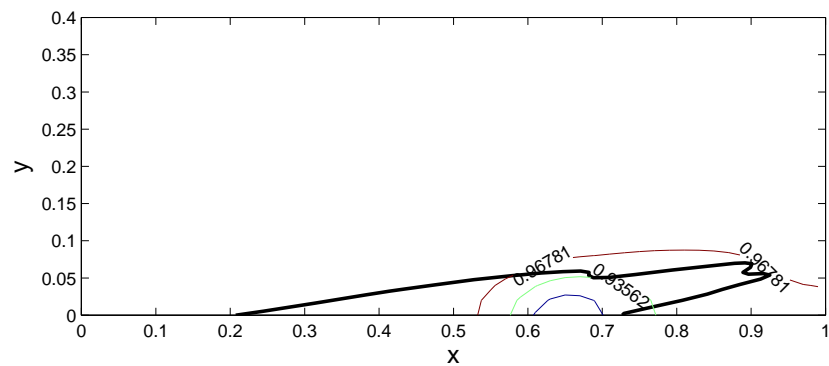


Figure 4: This shows a snapshot of the biofilm with viscosity $\mu = 500$ at time $t = 96(\text{min})$. The evolved interface is shown along with labeled contours of the nutrient levels. Here we see that the nutrient has almost fully penetrated the biofilm, the bacteria are all susceptible at close to their maximum rate.

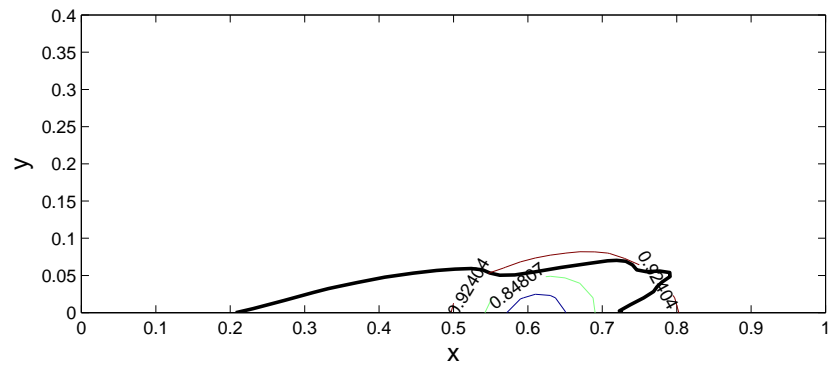


Figure 5: This shows a snapshot of the biofilm with viscosity $\mu = 1000$ at time $t = 96(\text{min})$. The evolved interface is shown along with labeled contours of the nutrient levels. We see that the nutrient has not penetrated as far as the simulation with $\mu = 500$ indicating that there is some level of protection being offered to the bacteria as seen in the survival curves in Figure 3.

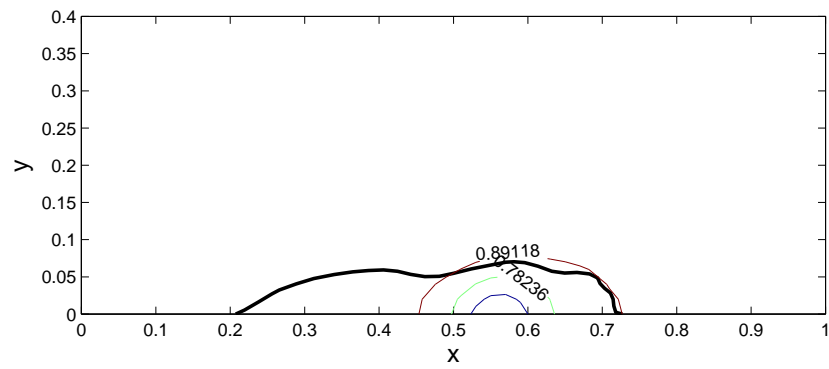


Figure 6: This shows a snapshot of the biofilm with viscosity $\mu = 5000$ at time $t = 96(\text{min})$. The evolved interface is shown along with labeled contours of the nutrient levels. Again, this is consistent with the results shown in Figure 3

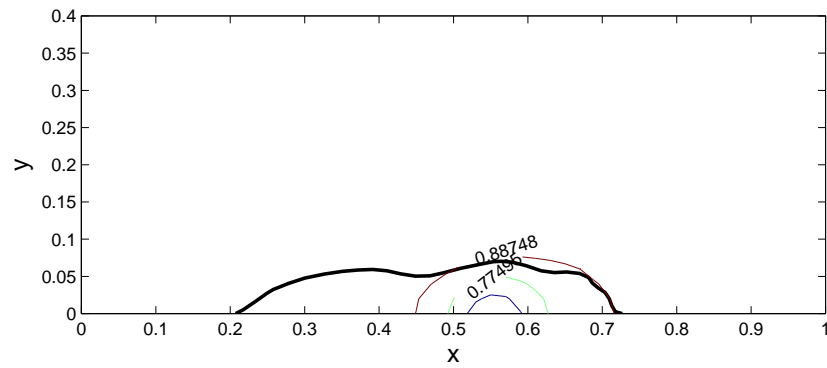


Figure 7: This shows a snapshot of the stationary biofilm at time $t = 96(\text{min})$. The interface is shown along with labeled contours of the nutrient levels.

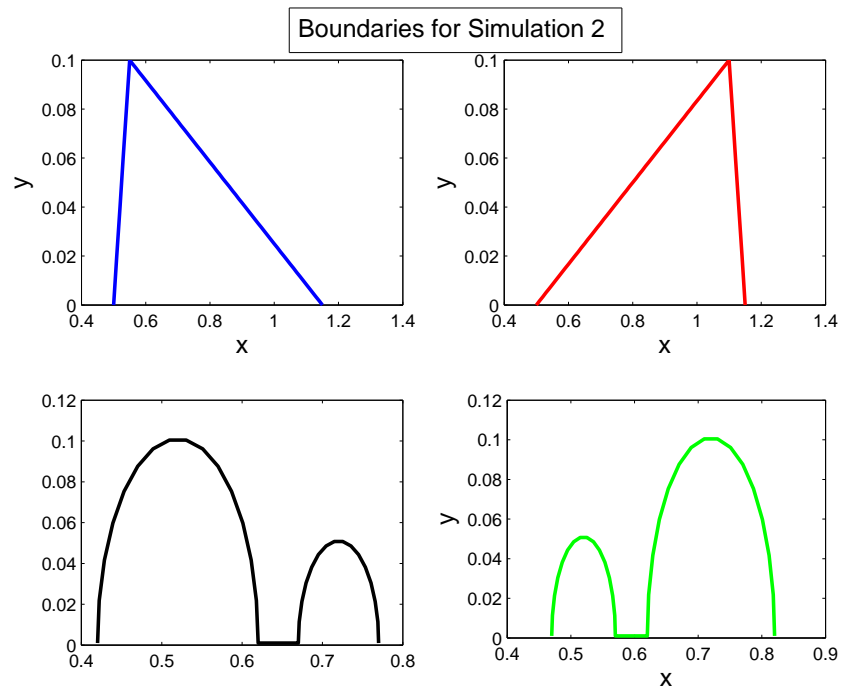


Figure 8: Initial domains for the second simulation set. The second column is the reverse orientation of the first column. We were interested to compare the disinfection curves for these regions for fixed viscosity

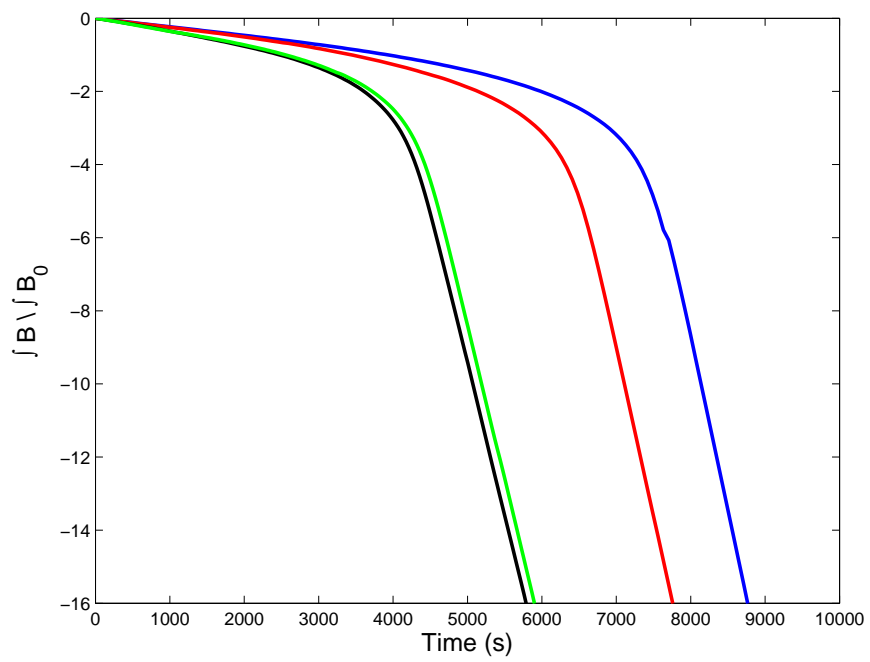


Figure 9: This shows the comparison of survival curves for the regions shown in Figure 8.

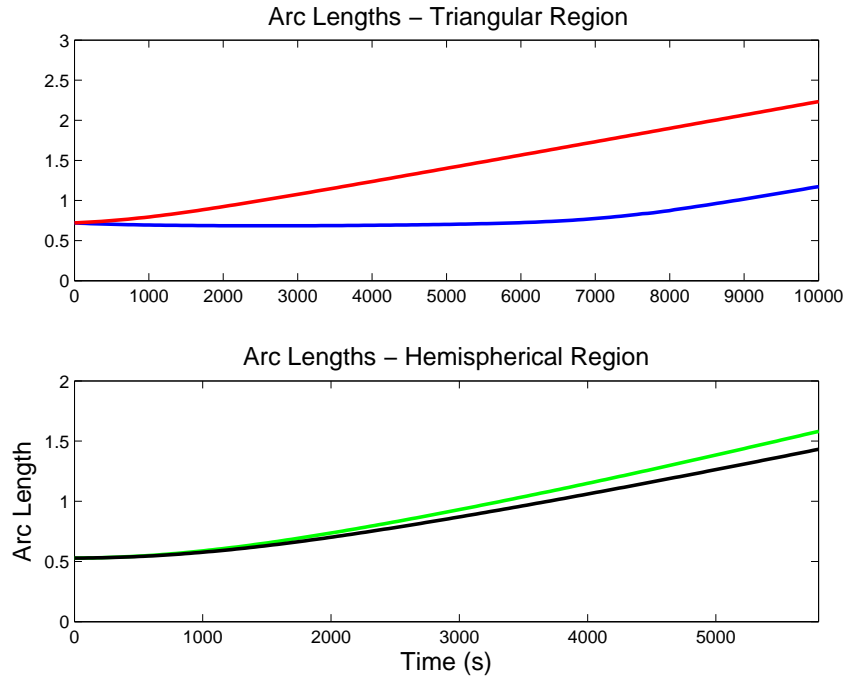


Figure 10: The arc length as a function of time for the regions in the second simulation set. The arc length was calculated numerically at each time step. The colors of the arc length curves correspond to the colors in Figure 8: blue - triangular 1, red - triangular 2, black - hemispherical (large first) and green - hemispherical (small first)

susceptible to disinfection. Comparing the triangular regions, we see that interface in the upper right has larger arc length and is more susceptible to disinfection.

Time Scale of Disinfection To try and understand this more fully, we considered methods to determine when the 'knee' of the disinfection curve occurs. The time at which the disinfection rate is maximal depends on the penetration time of the nutrient since the disinfectant rate depends on the nutrient availability and the biocide (which is constant in these simulations). To determine this time scale, we use the time course of nutrient concentration determined by the numerical simulations. We find the time at which the minimum values of the nutrient within the biofilm domain is .05 and .5 of the nutrient source concentration, $t_{.05}$ and $t_{.5}$ respectively. In Figure 11, we

indicate these times on the survival curves indicating that these times are covering the 'knee' of the curve for all our simulations.

Finally, we consider several other models of biofilm disinfection and compare the penetration times. In particular, we would like to determine the effects the motion of the biofilm region and the external flow have on the survival curves and penetration times. In [33], the author calculates the penetration time for various antimicrobial agents (e.g. nonreactive, reactive, sorbing) for a flat slab biofilm. Here there is no external flow. Instead the concentration of the biocide is constant at the interface. This can be upgraded to include a mass transfer boundary layer to incorporate the external flow in a qualitative manner.

We consider three simulations; the first is a numerical method similar to the analytic results in [33] where the bulk fluid is well mixed and there is no external flow, the second second incorporates explicit treatment of the external fluid with a fixed interface, and the final includes the motion of the biofilm and the external fluid. In each of these simulations the initial interface is a hemisphere of radius $.5$. As in the rest of the manuscript, our disinfection model allows us to track the nutrient concentration in order to track the disinfection of the biofilm. For the first simulation a boundary layer of the nutrient concentration is fixed at the interface and we consider diffusion of the nutrient into the biofilm. In the second simulation, we account for the motion of the external fluid while the biofilm region is fixed. In the third simulation, we allow for the biofilm to move as a viscous fluid with viscosity 500 times that of water. In Figure 12, we show the survival curves as well as the times at which the nutrient has penetrated to $.05$ and $.5\%$ of the source concentration. Again, we see that we are well able to capture the 'knee' of the survival curve. We also see that the pure diffusive case under-estimates the penetration times.

4 Discussion

We find that the disinfection is delayed as the biofilm viscosity increases. This suggests that if the viscosity of bacteria could be artificially increased, say by heating the substratum, disinfection might be aided. Because the disinfection of the bacteria is proportional to the growth rate, we also note that this implies that the less viscous biofilm has a lower overall growth rate than that of the fixed biofilm.

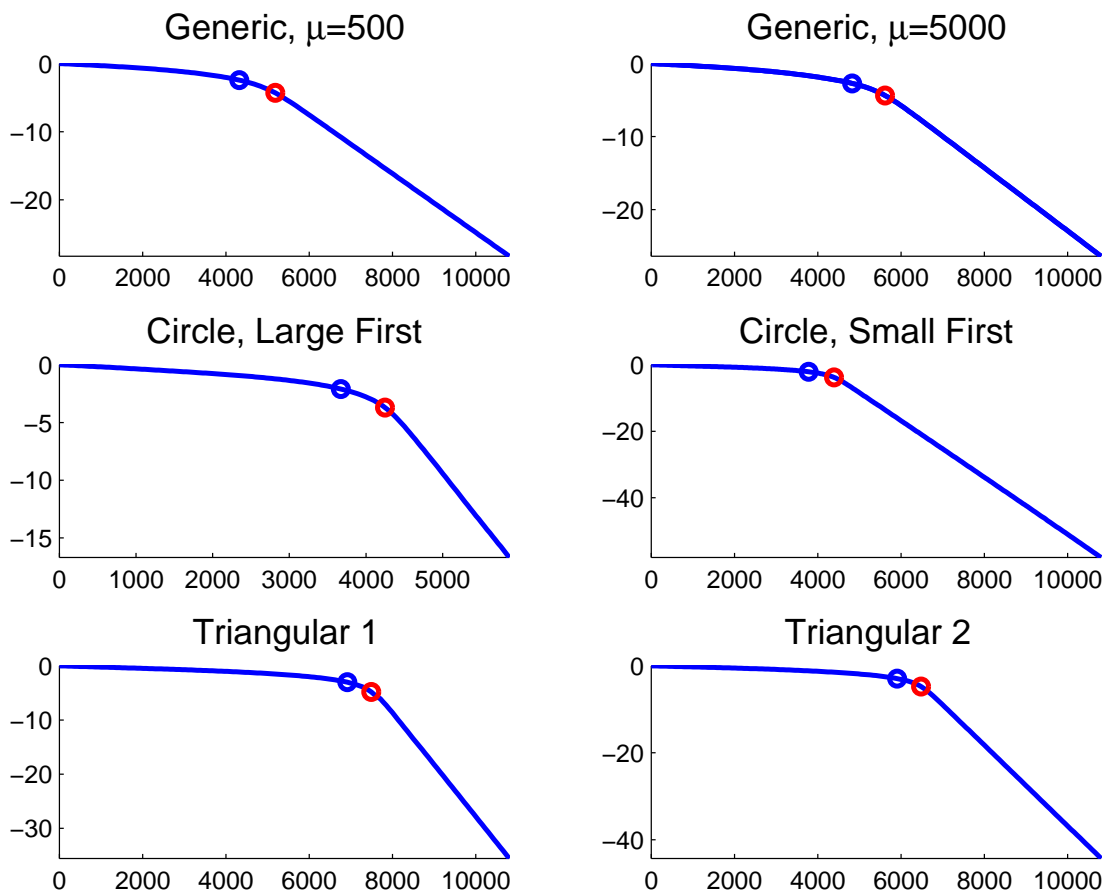


Figure 11: Survival curves with the time at which the nutrient has penetrated so that the minimum value within the biofilm region is .05, indicated by the blue circle, and .5, indicated by the red circle. This indicates a measure of the dependence of the disinfection on the penetration of the nutrient.

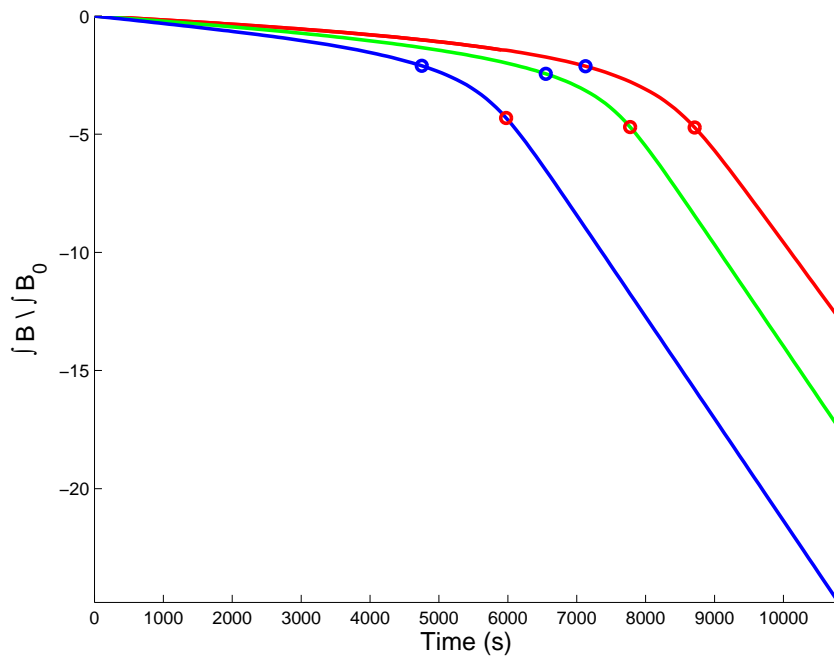


Figure 12: Survival curves for three simulations with the time at which the nutrient has penetrated so that the minimum value within the biofilm region is .05, indicated by the blue circle, and .5, indicated by the red circle. The survival curves for no external or internal flow (red), no internal flow (green) and both external and internal flows (blue) are shown.

We have also considered how the nutrient penetration time sets the maximum disinfection rate. This timescale is contrasted with other simplified models. In particular, we see that as the viscosity of the biofilm increases, the penetration time decreases. This indicates that although diffusion within the biofilm can delay the penetration of chemicals, neglecting the external and internal flows has a measurable effect on the estimate of penetration times.

References

- [1] N. Q. BALABAN, J. MERRIN, R. CHAIT, L. KOWALIK, AND S. LEIBLER, *Bacterial persistence as a phenotypic switch*, *Science*, 305 (2005), pp. 1622–1625.
- [2] G. BATCHELOR, *An Introduction to Fluid Dynamics*, Cambridge, U.P., 1967.
- [3] N. G. COGAN, *Effects of persister formation on bacterial response to dosing*, *Journal of Theoretical Biology*, (2005).
- [4] ———, *Hybrid numerical treatment of two-fluid problems with passive interfaces*, *SIAM Journal of Scientific Computing*, (2005). Submit.
- [5] N. G. COGAN, R. CORTEZ, AND L. J. FAUCI, *Modeling physiological resistance in bacterial biofilms*, *Bulletin of Mathematical Biology*, 67 (2005), pp. 831–853.
- [6] N. G. COGAN AND J. P. KEENER, *The role of the biofilm matrix in structural development*, *Mathematical Medicine and Biology*, 21 (2004), pp. 147–166.
- [7] R. CORTEZ, *The method of regularized stokeslets*, *SIAM J. Sci. Comput.*, 23 (2001), pp. 1204–1225.
- [8] R. CORTEZ, L. FAUCI, AND A. MEDOVNIKOV, *The method of regularized stokeslets in three dimensions: Analysis, validation, and application to helical swimming.*, *Phys. Fluids.*, 17 (2005), pp. 1–14.
- [9] J. COSTERTON, *Cystic fibrosis pathogenesis and the role of biofilms in persistent infection*, *Trends Microbiol.*, 9 (2001), pp. 50–52.
- [10] D. DAVIES, *Understanding biofilm resistance to antibacterial agents*, *Nature Reviews Drug Discovery*, 2 (2003), pp. 114–122.
- [11] M. DESAI, T. BUHLER, P. WELLER, AND M. BROWN, *Increasing resistance of planktonic and biofilm cultures of *Burkholderia cepacia* to ciprofloxacin and ceftazidime during exponential growth*, *Journal of Antimicrobial Chemotherapy*, 42 (1998), pp. 153–160.

- [12] R. DILLON AND H. G. OTHMER, *A mathematical model for outgrowth and spatial patterning of the vertebrate limb bud*, Journal of Theoretical Biology, 197 (1999), pp. 295–330.
- [13] M. G. DODDS, K. J. GROBE, AND P. S. STEWART, *Modeling biofilm antimicrobial resistance*, Biotechnology and Bioengineering, 68 (2000), pp. 456–465.
- [14] K. GROBE, J. ZAHLER, AND P. STEWART, *Role of dose concentration in biocide efficacy against Pseudomonas aeruginosa biofilms*, Journal of Industrial Microbiology and Biotechnology, 29 (2002), pp. 10–15.
- [15] M. HENTZER, H. WU, J. B. ANDERSEN, K. RIEDEL, T. B. RASMUSSEN, N. BAGGE, N. KUMAR, M. A. S. AND ZHIJUN SONG, P. KRISTOFFERSEN, M. MANEFIELD, J. W. COSTERTON, S. MOLIN, L. EBERL, P. STEINBERG, S. KJELLEBERG, N. HOIBY, AND M. GIVSKOV, *Attenuation of Pseudomonas aeruginosa virulence by quorum sensing inhibitors*, The EMBO Journal, 22 (2003), pp. 3803–3815.
- [16] T. Y. HOU, J. S. LOWENGRUB, AND M. J. SHELLEY, *Boundary integral methods for multicomponent fluids and multiphase fluids*, Journal of Computational Physics, 169 (2001), pp. 302–362.
- [17] I. KEREN, N. KALDALU, A. SPOERING, Y. WANG, AND K. LEWIS, *Persister cells and tolerance to antimicrobials*, FEMS Microbiology Letters, 230 (2004), pp. 13–18.
- [18] I. KLAPPER, C. RUPP, R. CARGO, B. PURVEDORJ, AND P. STOODLEY, *Viscoelastic fluid description of bacterial biofilm material properties*, Biotechnology and Bioengineering, 80 (2002), pp. 289–296.
- [19] H. M. LAPPIN-SCOTT AND J. W. COSTERTON, eds., *Microbial Biofilms*, Cambridge University Press, Cambridge, 1995, ch. Mechanisms of the Protection of Bacterial Biofilms from Antimicrobial Agents, pp. 118–130.
- [20] A. T. LAYTON, *An explicit jump method for the two-fluid stokes equations with an immersed elastic boundary*, Elsevier Science, (2006). Submitted.

- [21] R. J. LEVEQUE AND Z. LI, *The immersed interface method for elliptic equations with discontinuous coefficients and singular sources*, SIAM Journal of Numerical Analysis, 31 (1994), pp. 1019–1044.
- [22] R. J. LEVEQUE AND Z. LI, *Immersed interface methods for Stokes flow with elastic boundaries or surface tension*, SIAM J. Sci. Comput., 18 (1997), pp. 709–735.
- [23] K. LEWIS, *Riddle of biofilm resistance*, Antimicrobial Agents and Chemotherapy, 45 (2001), pp. 999–1007.
- [24] H. A. LORENZ, *Ein allgemeiner satz, die bewegung einer reibenden flussugkeit betreffend, nebst einigen anwendungen desselben*, Abhand. Theor. Phys., 1 (1907), pp. 23–42.
- [25] A. MAYO, *Fast high order accurate solution of Laplace’s equation on irregular regions*, SIAM J. Sci. Comput., 6 (1985), pp. 144–157.
- [26] R. MITTAL AND G. IACCARINO, *Immersed boundary methods*, Annual Review of Fluid Mechanics, 37 (2005), pp. 239–261.
- [27] C. POZRIKIDIS, *Boundary integral and singularity methods for linearized viscous flow*, Cambridge University Press, 1992.
- [28] ———, *Interfacial dynamics for stokes flow*, Journal of Computational Physics, 169 (2001), pp. 250–301.
- [29] ———, *Modeling and Simulation of Capsules and Biological Cells*, Chapman & Hall/CRC Press., 2003.
- [30] B. PRAKASH, B. VEEREGOWDA, AND G. KRISHNAPPA, *Biofilms: A survival strategy of bacteria*, Current Science India, 85 (2003), pp. 1299–1307.
- [31] M. E. ROBERTS AND P. S. STEWART, *Modeling antibiotic tolerance in biofilms by accounting for nutrient limitation*, Antimicrobial Agents and Chemotherapy, 48 (2004), pp. 48–52.
- [32] S. S. SANDERSON AND P. S. STEWART, *Evidence of bacterial adaption to monochloramine in Pseudomonas aeruginosa biofilms and evaluation of biocide action model*, Biotechnology and Bioengineering, 56 (1997), pp. 201 – 209.

- [33] P. S. STEWART, *Theoretical aspects of antibiotic diffusion into microbial biofilms*, *Antimicrobial Agents and Chemotherapy*, 40 (1996), pp. 2517–2522.
- [34] N. SUFYA, D. ALLISON, AND P. GILBERT, *Clonal variation in maximum specific growth rate and susceptibility towards antimicrobials*, *Journal of Applied Microbiology*, 95 (2003), pp. 1261–1267.
- [35] W. T. VETTERLING, S. A. TEUKOLSKY, W. H. PRESS, AND B. FLANNERLY, *Numerical Recipes in C: The Art of Scientific Computing*, Cambridge University Press, Cambridge, 2002.